

Canadian Journal of Pure and Applied Sciences
Vol. 9, No. 2, pp. 3519-3534, June 2015
Online ISSN: 1920-3853; Print ISSN: 1715-9997
Available online at www.cjpas.net



Canadian Journal of
pure & applied
sciences

SYNTHESIS OF (*E*)-*N'*-(5-bromo-2-hydroxybenzylidene)nicotinohydrazide) AND ITS Pt(II), Zn(II), Mn(II), Ni(II) AND Mo(V) COMPLEXES AS POTENTIAL ANTI-TUBERCULAR AGENT

*KO Ogunniran¹, MA Mesubi², JA Adekoya¹, OO Siyanbola¹, AI Inegbinebor¹, OO Ojo³, AE Adedapo¹, A Edobor-Osoh¹ and T Narender⁴

¹Department of Chemistry, College of Science and Technology, Covenant University, Ota, Ogun State, Nigeria

²Department of Chemistry, Kwara State University, Molete, Kwara State, Nigeria

³Department of Biochemistry, Ekiti State University, Ado-ekiti, Nigeria

⁴Medicinal and Process Chemistry Division, CSIR-Central Drug Research Institute, Lucknow, India

ABSTRACT

The cold condensation reaction of nicotinic acid hydrazide and 5-bromo-2-hydroxybenzaldehyde to form a tridentate Schiff base hydrazone ligand (H_2L^3) was studied. The prepared ligand was characterized using CHN analyzer, ESI mass spectrometry, IR, ¹H NMR, ¹³C NMR and 2D NMR such as COSY and HSQC. Thereafter, five novel metal complexes [Pt(II), Zn(II), Mn(II), Ni(II) and Mo(V)] of the hydrazone ligand were synthesized and characterized based on conductivity measurements, CHN analysis, AAS, magnetic measurement, UV/Vis, IR, ESR and TGA/DTA study. The proposed structures of the metal complexes were further supported with the use of powder X-ray analysis. Anti-tubercular activity study of the compounds was evaluated against *Mycobacterium tuberculosis* H37Rv by using micro-diluted method. The study revealed that H_2L^3 exhibited promising anti-tubercular activity with MIC value of 0.82 $\mu\text{g/mL}$. Also, metal complexes ([Pt(H_2L^3)Cl]- 0.88 $\mu\text{g/mL}$, [Mn(H_2L^3)(CH₃COO)₂]- 0.78 $\mu\text{g/mL}$, [Zn(H_2L^3)(CH₃COO)₂H₂O]- 0.62 $\mu\text{g/mL}$ and [Ni(H_2L^3)(Cl)₂H₂O]- 1.19 $\mu\text{g/mL}$) exhibited significant inhibition as compared to the standard drug (isoniazid- 0.91 $\mu\text{g/mL}$). Complex **2** and **3** with coordinated acetates showed two folds inhibition than standard isoniazid drug. However, complex **5** with coordinated chlorine atom displayed lower inhibition when compared to isoniazid.

Keywords: X-ray, hydrazones, metal complexes, electron spin resonance, thermogravimetric, crystallographic, antitubercular agents.

INTRODUCTION

The world is presently facing challenges of various types of epidemic diseases. Efforts are being made by Scientists all over the world to find new compounds that could be used successfully to tackle problems of drug resistance. The field of bioinorganic chemistry offered better chance in this area. The metal complexes of acylhydrazone have been recognized to serve as models for biologically important species (Rakesh *et al.*, 2009; Jia *et al.*, 2005). Based on this, there have been sudden interests in the study of metal complexes of acylhydrazones in the last decade. Reports have shown that most of the compounds have enhanced biological properties, such as anti-inflammatory, analgesic, anticonvulsant, antitubercular (Lourenço *et al.*, 2008; Dharmaraj *et al.*, 2012) antitumor (Andreani *et al.*, 2008), anti-HIV (Rollas and Kucukguzel, 2007) and antimicrobial activity (Banerjee *et al.*, 2009; Shi *et al.*, 2007). Tuberculosis (TB) is a highly

infectious disease that is caused mainly by *Mycobacterium tuberculosis*. It is one of the diseases that require urgent attention across the world due to the fact that it kills between 2 and 3 million people every year (Lourenço *et al.*, 2008; Aboul-Fadel *et al.*, 2010). Most of the victims of TB are mainly in Asian and African countries where about 70-80% of the populations are infected (Kaufmann and Parida, 2008). Tuberculosis cases have been a burden to a number of countries in the world. The top five TB infected ranking countries are; India, China, Indonesia, South Africa, and Nigeria (Harper, 2009; Laughon, 2007). The situation has become more complicated due to increases in multidrug-resistant (MDR) TB (WHO, 2010). Based on the alarming rate, it was estimated that 0.22 billion people may acquire TB and 79 million could die due to TB by the year 2030.

Treatment of TB takes longer time due to the unusual structure and chemical composition of the *Mycobacterial*

*Corresponding author e-mails: kehinde.ogunniran@covenantuniversity.edu.ng

cell wall, which resisted many antibiotics and also hinders the entry of drugs (Jia *et al.*, 2005). The standard DOTS course (Directly Observed Treatment Short course) for TB is a 6 months treatment (Jindani *et al.*, 2004). Most of the current drugs for the treatment of TB resulted from the research performed over half a century ago (Sacchettini *et al.*, 2008). Hence, there is an urgent need to develop more potent and fast acting anti-TB drugs with new modes of action to overcome the cross-resistance with current drugs and with low toxicity profiles that can be tolerated for long treatment periods (Salib *et al.*, 2003). Presently, some drugs are under clinical trial by several public and private partnerships (Dover and Coxon, 2011). Despite the severe outbreak of TB and the rise of MDR strains, progress to find a new vaccine or improvement of the BCG vaccine has been very slow. Several numbers of approaches such as target-based drug design, combinatorial synthesis, high-throughput screening, etc., have been explored to generate new novel compounds. However, chemical modification of a known anti-TB drug has been reported to be a successful approach in the development of new anti-TB agent (Ramon-Garcia *et al.*, 2011). The present study is focus on the synthesis and characterization of the hydrazone obtained in the condensation reaction of nicotinic hydrazide with 5-bromosalicylaldehyde and its Pt(II), Zn(II), Mn(II), Ni(II) and Mo(V) complexes. The structure of the ligand was established with the use of some spectroscopy study while the structures of the metal complexes were proposed. The *in vitro* anti-tubercular activity against resistant strains of H37Rv was carried out to determine the anti-tubercular potential of the compounds.

MATERIALS AND METHODS

Nicotinic hydrazide, 5-bromosalicylaldehyde, PtCl_2 , $\text{Zn}(\text{COOCH}_3)_2$, $\text{Mn}(\text{COOCH}_3)_2 \cdot 4\text{H}_2\text{O}$, $\text{NiCl}_2 \cdot 4\text{H}_2\text{O}$, MoCl_5 and solvents with high purity were purchased from Sigma-Aldrich. They are of high purity and were used as purchased.

The melting points of all the compounds were determined by using Gallenkamp melting point apparatus (Davidson, 2010). The % of carbon, nitrogen and hydrogen in the synthesized hydrazones and metal complexes were determined by using Vario EL CHNS analyser at Sophisticated Analytical Instruments Facilities at Central Drug Research Institute, Lucknow, India. ESI-MS spectrum for the hydrazone was collected from Agilent 6520 Q-TOF mass spectrometer and MeOH solution was used as the solvent. Mass spectra were measured in positive mode and in the range $m/z = 200-1400$. The percentage of metal in the synthesized metal complexes was determined by using Varian spectrometer AAS-110. The molar conductivities of the metal complexes at ambient temperature in DMF solution (10^{-3}M) were measured using systronics – 304 conductivity meter. The

electronic data of the hydrazone and the metal complexes were obtained in methanol/DMSO by using Perkin Elmer Spectro UV-visible Double Beam UVD spectrometer in the range of 200-700 nm. The infrared spectra for the hydrazone and the metal complexes were recorded on Perkin – Elmer RX-1 Fourier Transform Infrared Spectrometer using KBr pellets in the range of 400-400 cm^{-1} . ^1H NMR, ^{13}C NMR and 2D NMR (COSY and HSQC) spectra of the hydrazone were recorded by using Bruker AMX 300 FT-NMR spectrometer in DMSO- d_6 . The magnetic susceptibility data of the paramagnetic metal complexes were measured at room temperature by using vibrating susceptibility magnetometer (PAR 155) with magnetic field of -10 to +10 kOe at instrumentation center, Indian Institute of Technology, Roorkee, India. TGA/DTA analyses of the metal complexes were carried out, at heating rate of $10\text{ }^\circ\text{C min}^{-1}$, under inert atmosphere by using thermogravimetric analyser TGA Q500 V20.8 Build 34 model. The EPR spectra of the metal complexes at 77 K were recorded on a Varian E-112 spectrometer using TCNE as the standard, with 100 KHz modulation frequency, modulation amplitude 2G and 9.1 GHz microwave frequency. X-ray powder diffraction pattern for Ni(II) complex was recorded on a Bruker AXS D8 Advance diffractometer operating in the θ/θ mode and equipped with a secondary beam graphite monochromator.

Synthesis of the hydrazone

The synthetic methods described earlier (Nair, 2012; Abeda, 2012) were modified and adopted. The nicotinic acid hydrazide (10 mmol, 342 mg) was dissolved in 20 ml absolute ethanol by heating gently on water bath. The solution of nicotinic acid hydrazide was mixed with 20 ml ethanolic solutions of 5-bromosalicylaldehyde (10 mmol, 503 mg) in a round bottom flask after which the mixture was stirred at 20°C for 6 h (Scheme 1). The precipitates obtained were allowed to stay at room temperature for 12 h before they were filtered, and washed with 30 ml of ethanol thrice. The compound obtained was recrystallized in mixture of dried chloroform. Vacuum pump rotary evaporator was used to ensure complete dryness. The purity was checked by TLC (10% methanol: 90% chloroform).

Yield 2.52 g (78%); milky colour solid; mp: $220-222^\circ\text{C}$; $R_f = 0.82$ ($\text{CHCl}_3 / \text{CH}_3\text{OH}$, 4:1, at RT.). IR (KBr) cm^{-1} : 3418 (ArOH), 3266 (NH), 1675 (C=O), 1610 (C=N), 1529 (N-N), 1339 (C-O), 1147(C-N). MS (ESI+): in m/z : 320.0 $[\text{M} + \text{H}]^+$. Anal. calcd. for $\text{C}_{13}\text{H}_{10}\text{BrN}_3\text{O}_2$ (319.00): C, 48.90; H, 3.13; N, 13.16. Found: C, 48.76; H, 3.47; N, 12.78. $^1\text{H-NMR}$ (DMSO- d_6) δ : 12.32(s, 1H, NH), 11.19 (s, Ar-OH, 1H), 9.08 (d, $J_1 = 1.2$ Hz, 1H, H(3)), 8.78 (dd, $J_1 = 4.8$ Hz, $J_2 = 7.9$ Hz, 1H, H(4)), 8.61 (s, 1H, H-C=N), 8.29 (dt, $J_1 = 1.5$ Hz, $J_2 = 8.1$ Hz, 1H, H(6)), 7.81 (d, $J = 2.4$ Hz, 1H, H(7)), 7.59 (m, $J_1 = 4.8$ Hz, $J_2 = 8.1$ Hz, 1H, H(8)), 7.44 (dd, $J_1 = 2.4$ Hz, $J_2 = 8.7$ Hz, 1H, H(9)), 6.92

(d, $J = 8.7$ Hz, 1H, H(10), ppm. $^{13}\text{C-NMR}$ (DMSO- d_6) δ : 162.56 (CO), 156.40 (C-OH), 152.41 (C3), 148.60 (C4), 146.03 (HC=N), 135.45 (C6), 133.71 (C7), 130.26 (C8), 128.53 (C9), 123.57 (C10), 121.19 (C11), 118.63 (C12), 110.47 (C13), ppm.

Synthesis of the metal complexes

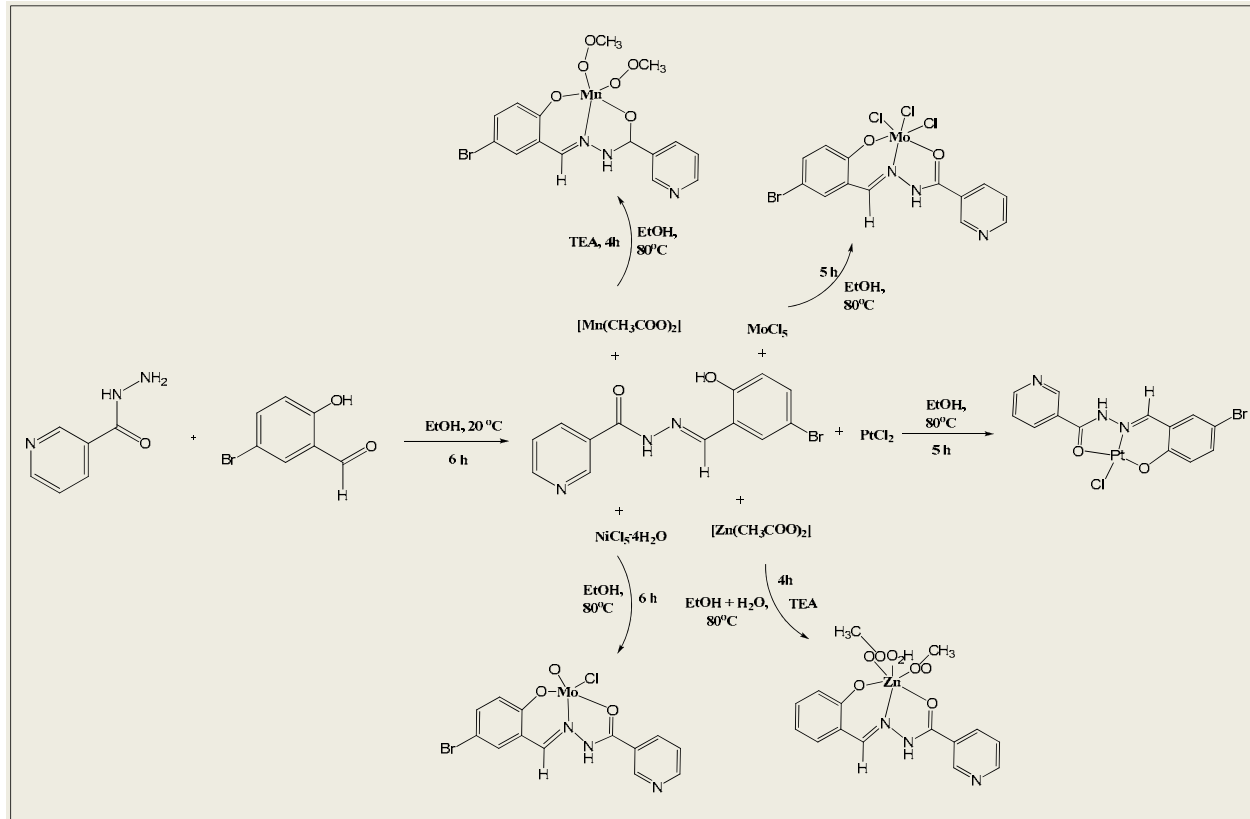
[Mn(H₂L³)(CH₃COO)₂]: To an ethanolic solution of H₂L³ (10 mmole, 161 mg), 10 mmole (153 mg) of [Mn(CH₃COO)₂·4H₂O] dissolved in 20 ml of ethanol was added slowly after which 2 drops of TEA was added. The mixture was refluxed at 80°C for 4 h. The brown product formed was filtered, washed with ethanol followed by ether and dried over P₄O₁₀ in vacuo. Elemental Anal. found (Calcd.) (%): Mn, 10.73 (11.14); C, 41.16 (41.40); H, 2.84 (3.27); N, 9.23 (8.52). $\mu = 5.54$ BM.

[Zn(H₂L³)(CH₃COO)₂·H₂O]: 229 mg (10 mmole) of Zn(CH₃COO)₂ was dissolved in 10 ml of mixture of ethanol and distilled water (1:1). The solution obtained was added gradually to 400 mg ethanolic solution of H₂L³ (10 mmole in 10 ml of absolute ethanol) in a round bottom flask after which two drops of TEA was added. The solution was refluxed at 80°C for 4 h. The yellow precipitate formed was allowed to cool to ambient temperature after which it was filtered, washed with 15 ml of ethanol and then with 10 ml of ether. The precipitate

obtained was dried by using vacuum rotary evaporator. Elemental Anal. found (Calcd.) (%): Zn, 13.01 (12.54); C, 39.25 (39.14); H, 3.37 (3.48); N, 8.23 (8.06). $\mu = 0$ BM.

[Pt(H₂L³)Cl]: 166 mg (10 mmole) of PtCl₂ dissolved in 10 ml of absolute ethanol was added to 400 mg (10 mmole) of H₂L³ dissolved in 10 ml of absolute ethanol. The mixture was refluxed at 80 °C for 5 h after which it was left at room temperature for 24 h during which green precipitates formed. The precipitate formed was filtered, washed with cold ethanol and then dried over P₄O₁₀ in vacuo. Yield: 0.189 g (54.93 %). Elemental Anal. found (Calcd.) (%): M, 34.78 (35.43); C, 27.65 (28.35); H, 2.15 (1.83); N, 7.96 (7.63). $\mu = 0$ BM.

[Ni(H₂L³)(Cl)₂]H₂O: 149 mg (10 mmole) of NiCl₂·4H₂O dissolved in 10 ml of absolute ethanol was added to 20 ml ethanolic solution of H₂L³ (800 mg, 20 mmole) in a round bottom flask after which two drops of TEA was added. The solution was refluxed at 80 °C for 6 h. The precipitate formed was filtered, washed with 20 ml of ethanol and then with 10 ml of ether. The precipitate obtained was dried over P₄O₁₀ in vacuo. Elemental Anal. found (Calcd.) (%): Ni, 13.23 (12.55); C, 32.69 (33.38); H, 2.12 (2.59); N, 8.59 (8.98). $\mu = 3.53$ BM.



Scheme 1. Synthetic pathway for H₂L³ and its metal complexes.

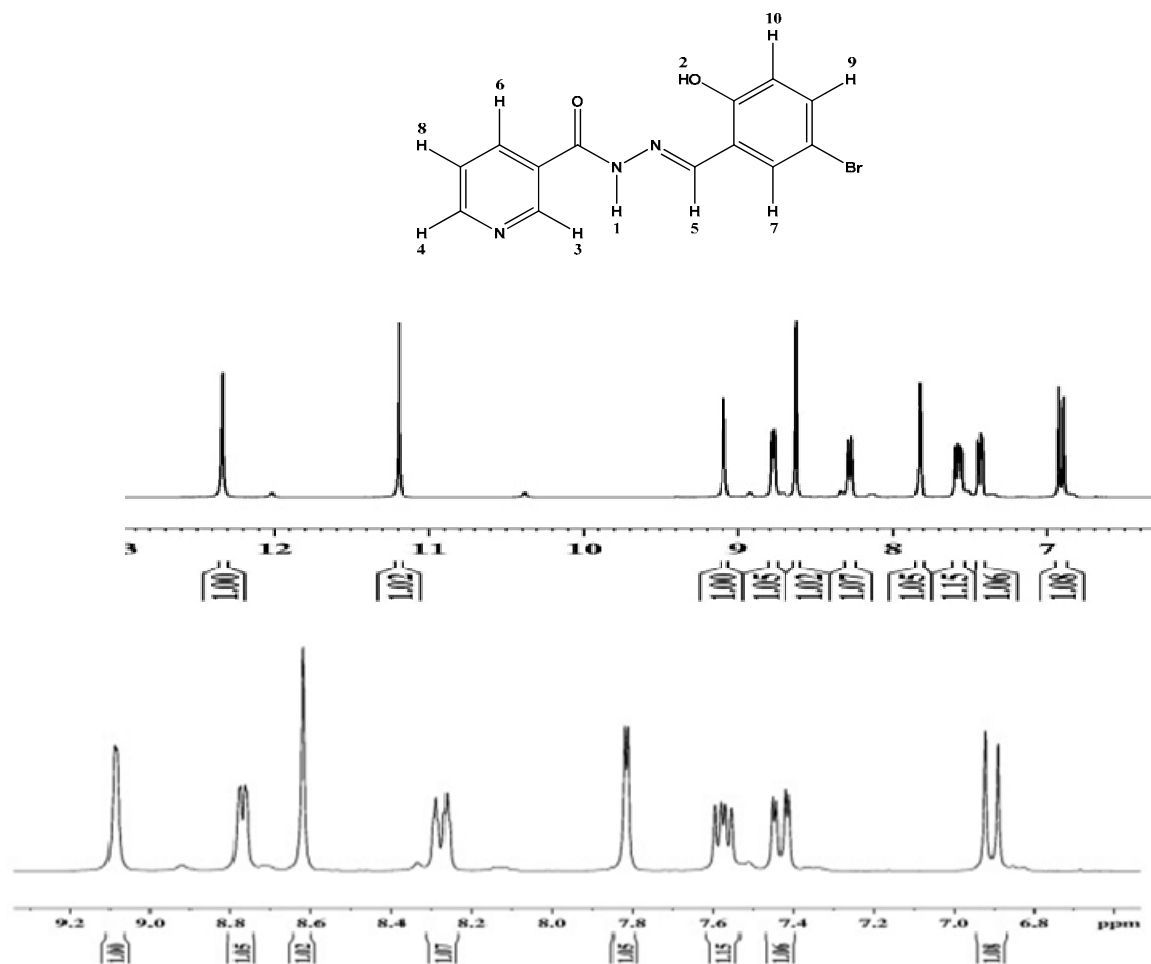


Fig. 1. ^1H NMR spectrum of H_2L^3 in DMSO-d_6 at 300 MHz.

$[\text{Mo}(\text{H}_2\text{L}^3)_2(\text{Cl})_3]$: Equivalent of 10 mmole (171 mg) of MoCl_5 was weighed into appendorf in a fumes cupboard and transferred directly into the 10 ml of absolute ethanol in a double neck round bottom flask. The appendorf was rinsed into the solution with 5 ml of ethanol. Then solution of (400 mg, 10 mmole) of H_2L^3 in 15 ml of absolute ethanol was added. The mixture was refluxed at 80°C for 5 h under nitrogen gas. The solute obtained was filtered, washed with cold ethanol and dried over P_4O_{10} in vacuo. Yield: 0.187 g (57.36%). Elemental Anal found (Calcd.) (%): Mo, 17.95 (18.36); C, 30.36 (29.89); H, 2.43 (1.93); N, 7.97 (8.04). μ = not determined BM.

Antimycobacterial Activity Study

MIC determination

The synthesized hydrazone and metal complexes were evaluated for *in vitro* anti-mycobacterial activity. The compounds were screened against *M. tuberculosis* H37Rv in triplicate using broth dilution method (Anna, 2009;

Gopalakrishnan, 2008). The compounds were screened against isoniazid (ATCC 35822) resistant strains of *M. tuberculosis*. The compounds were serially diluted from concentration of $500\ \mu\text{g}/\text{mL}$ to $25\ \mu\text{g}/\text{mL}$ in DMSO. *M. tuberculosis* H37Rv strain was used in Middle brook 7H-9 broth which was inoculated with standard as well test compounds and incubated at 37°C for 4 weeks. The bottles were inspected for growth trice a week for a period of three weeks. Readings were taken at the end of 4 weeks. The appearance of turbidity was considered as growth and indicates resistance to the compound. The growth was confirmed by making a smear from each bottle and performing a ZN stain.

RESULTS AND DISCUSSION

The reaction of nicotinic acid hydrazone with 5-bromosalicylaldehyde (see Scheme 1) gave the desired dissymmetric tridentate Schiff base hydrazone in high

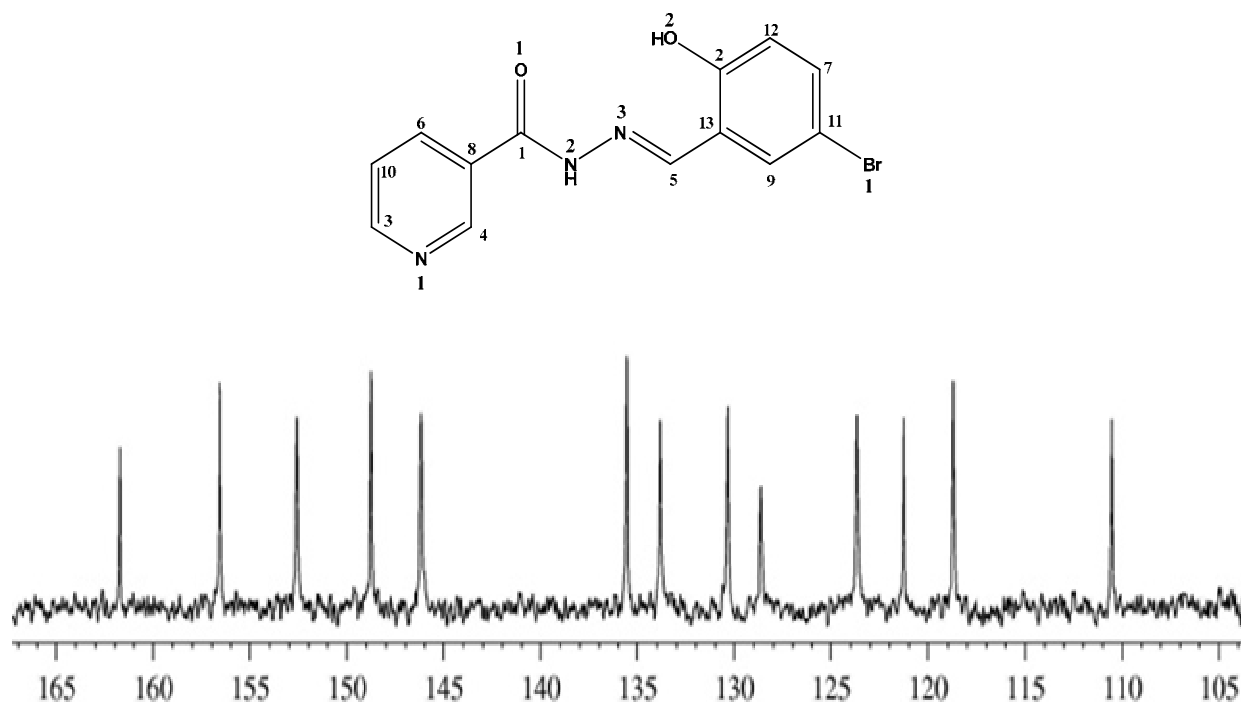


Fig. 2. ^{13}C NMR spectrum of H_2L^3 in $\text{DMSO-}d_6$ at 75 MHz.

yield and purity. The ESI mass spectrum (Supplementary 1) for the compound confirmed the molecular mass of the compound with molecular ion peak ($M + 1$) at 320.2. The molecular ions peak observed was supported by micro analysis data obtained.

^1H NMR spectrum study

The ^1H NMR spectrum of the compound in $\text{DMSO-}d_6$ (Fig. 1) displayed singlet peak which was assigned to an imine proton, H(1) in the hydrazone at 12.32 ppm. It resonated down the field due to highly deshielding effect from N(2) atom. This assignment was confirmed by deuterium exchange in which the intensity of this band decreased considerably (Devidas *et al.*, 2011; Parekh *et al.*, 2005). The singlet peak at 11.19 ppm corresponded to hydroxyl proton H(2), which was highly de-shielded by attached oxygen atom. In the pyridyl ring, the two adjacent protons, H(3) and H(4), to nitrogen atom N(1) appeared downfield at 9.08 and 8.78 ppm. However, the peak at 9.08 ppm is a doublet peak while the peak at 8.78 ppm appeared as doublet of doublet. The two peaks experienced hydrogen bonding from neighboring nitrogen atom and thus resonated downfield. The multiplet peak at 7.59 ppm which integrated as one proton, was assigned to H(8) protons. The doublet of triplet peak at 8.29 ppm was assigned to H(6) proton. The singlet peak which integrated as one proton at 8.61 ppm was assigned to H(5)

proton in the hydrazone. The proton experienced high reduction in the electron density around it from the adjacent nitrogen atom N(3). The two peaks observed at 7.81 and 7.44 ppm were assigned to H(7) and H(9) protons respectively. High δ values for the two protons are based on their ortho position to bromine atom in the phenol ring. H(10) proton in the phenol ring was assigned to a doublet peak that resonated at 6.92 ppm.

^{13}C NMR spectrum study

^{13}C NMR spectrum (Fig. 2) confirmed thirteen carbon atoms in the hydrazone ranging from 110.47 to 161.56 ppm as envisaged. The carbonyl carbon C(1) appeared downfield at 161.56 ppm due to its direct attachment to oxygen that reduced its electron density. The observation was coupled with conjugative effect from N(2)-N(3) core in the hydrazone. The peak at 156.40 ppm was assigned to the carbon C(2) attached to hydroxyl group in the molecule. The downfield position is partially due to inter-hydrogen bonding experienced by the OH group (Pavia *et al.*, 2008). In the pyridyl ring, the two carbon atoms adjacent to N(1), C(3) and C(4), resonate at lower field of δ 152.41 ppm and 148.60 ppm, respectively. The other carbon atoms in the pyridyl ring are C(6), C(8) and C(10). They were assigned to the peak at 135.45, 130.26 and 123.57 ppm respectively. The resonances assigned to the

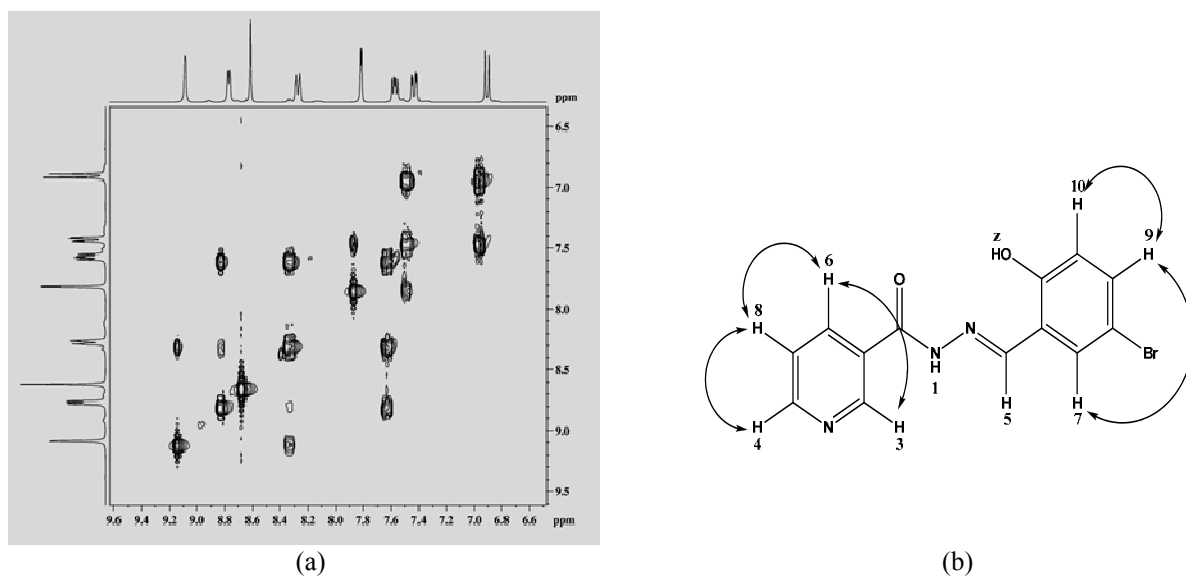


Fig. 3. COSY spectrum and schematic structure for H_2L^3 recorded in $DMSO_{d6}$ at 300 MHz.

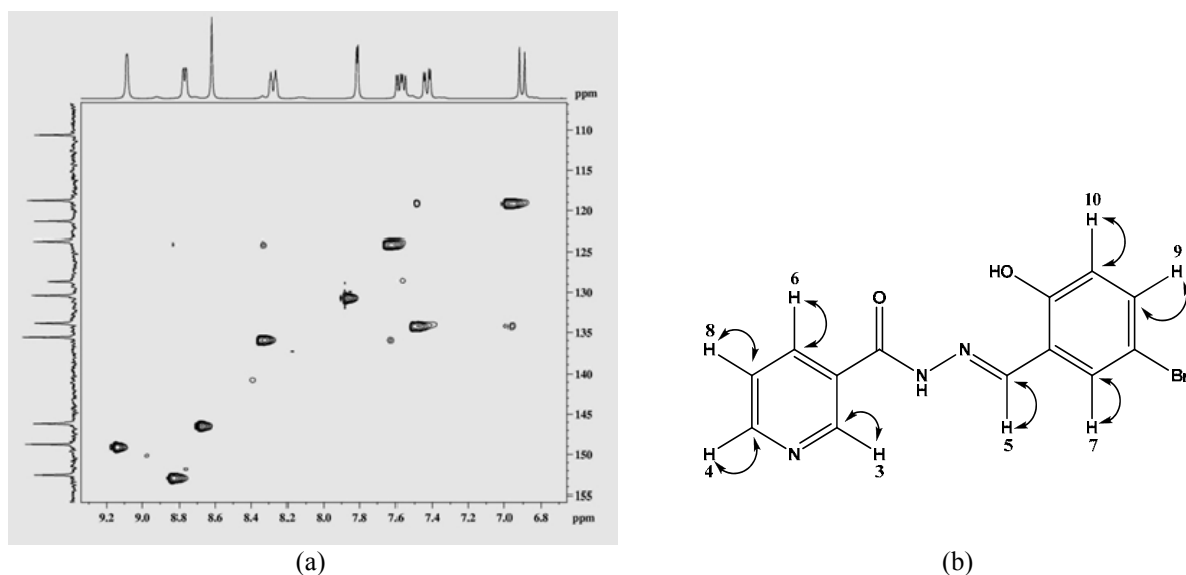


Fig. 4. HSQC spectrum and schematic diagram for H_2L^3 recorded in $DMSO-d_6$ at 75 MHz.

carbon atoms in the phenol ring are C(7) 133.71; C(9) 128.53; C(11), 121.19; C(12) 118.63 and C(13) 110.47 ppm. The carbon atom attached to Br atom, C(9), appeared at much lower field than other carbon because it experienced much reduction in its electron density than the other carbons. However, C(5) atom was assigned to the peak that resonated downfield at 146.03 ppm. The peak appeared at the lower field due to high de-shielding effect from adjacent N(3)-N(2) core of the hydrazone.

COSY spectrum study

1H - 1H correlation spectroscopy confirmed the assignments of proton NMR spectrum. There was no correlation for the peaks at 12.32, 11.19 and 8.61 ppm, which confirmed the absence of coupling interaction for

each of these protons with their neighboring protons in the molecule. However, off diagonal contours were observed in the pyridyl ring and phenol ring region. The proton atom at 7.59 ppm, assigned to H(8), experienced coupling effect from both H(6) at 8.29 ppm and H(4) at 8.78 ppm. Also, the peak at H(6) correlated with the peak at 9.08 ppm, H(3) and this account for the doublet of triplet peak at 8.39 ppm assigned to H(6). The peak at 7.59 ppm appeared as multiplet due to two *ortho* coupling experienced while the peak at 8.78 ppm appeared as doublet of doublet peak. In the phenol ring region, the proton at 7.44 ppm which was assigned to H(9) proton correlate with both H(7) proton at 7.81 ppm and H(10) at 6.92 ppm. Therefore, this justified doublet of doublet peak observed at 7.44 ppm while both H(7) and H(10)

Table 1. Analytical data of H₂L³ metal complexes.

Complex	Colour	M. pt. °C	Found (Calc.), %				Λ_M S cm ² mol ⁻¹	μ_{eff} μB
			M	C	H	N		
[Mn(H ₂ L ³)(CH ₃ COO) ₂] (2)	Yellow	300	10.73 (11.14)	41.16 (41.40)	2.84 (3.27)	9.23 (8.52)	35	5.54 (5.92)
[Zn(H ₂ L ²)(CH ₃ COO) ₂ H ₂ O] (3)	Yellow	300	13.01 (12.54)	39.25 (39.14)	3.37 (3.48)	8.23 (8.06)	48	-
[Pt(H ₂ L ³)Cl] (4)	green	300	34.78 (35.43)	27.65 (28.35)	2.15 (1.83)	7.96 (7.63)	28	-
[Ni(H ₂ L ³)Cl ₂]H ₂ O (5)	Golden yellow	300	13.23 (12.55)	32.69 (33.38)	2.12 (2.59)	8.59 (8.98)	43	3.53 (2.83)
[Mo(H ₂ L ³)Cl ₃] (6)	Black	300	17.95 (18.36)	30.35 (29.89)	2.43 (1.93)	7.97 (8.04)	38	-

protons resonated as doublet peaks. Based on this, ¹H-¹H coupling for the hydrazone is shown in figure 3b.

HSQC spectrum study

The ¹H-¹³C HSQC correlation spectrum which was recorded in DMSO-d₆ ascertained both ¹H and ¹³C NMR assignments. The ¹H-¹³C HSQC connectivity in this spectrum is in agreement with both ¹H and ¹³C spectral assignments. From the HSQC spectrum (Fig. 4), the peaks at 161.56, 156.40, 130.26, 121.19 and 110.47 ppm assigned to C(1), C(2), C(8), C(11) and C(13) respectively did not show correlation with any of the proton in the hydrazone. This confirmed that they are non-protonated carbons. However, HSQC spectrum showed 8 protonated carbons as expected for the molecule. All the correlation observed matched the ¹H and ¹³C NMR assignments. Based on the spectrum, the H-C correlation scheme is shown in figure 4.

Analytical data of the metal complexes

The synthesized metal complexes of H₂L³ possess characteristics colour with high melting point (>300°C) due to the coordination bonds (Table 1). They were found to be sparingly soluble in methanol, DMF and THF but were soluble in DMSO and pyridine. The results of elemental analyses (C, H, N) obtained are in good agreement with the calculated values. The magnetic susceptibility values recorded at room temperature for Mn(II) and Ni(II) complexes compete favorably with the calculated spin only magnetic values. The conductivity values of the metal complexes are very low, thus suggesting non-electrolytic character of the metal complexes.

Infra-red spectra studies

The infrared spectral assignments of H₂L³ compared to its metal complexes are presented in table 2. The comparison of the infrared spectrum of H₂L³ with the spectra of the metal complexes, figure 5, showed significant variation in the chromophoric absorption bands due to the effect of coordination. The broad band around 3418 cm⁻¹ which

was assigned to ν(OH) stretching modes in H₂L³ was observed in the spectra of Zn(II), Pt(II) and Mo(V) complexes at higher wavenumbers (3419-3456 cm⁻¹), coupled with increased broadness. This observation was attributed to the effect of coordination of the oxygen atom of the OH group after deprotonation (Kuriakose *et al.*, 2007). Also, Ni(II) and Mn(II) complexes showed ν(M-O) absorption band at lower wavenumbers with reduction in its intensity due to presence of intra-molecular hydrogen bond in the two complexes.

The strong band at 1675 cm⁻¹ attributed to ν(C=O) vibrational stretching mode in H₂L³ appeared in the spectra of the metal complexes at lower wavenumber from 1606 cm⁻¹ in Mn(II) complex to 1655 cm⁻¹ in Pt(II) complex. The intensities of the peaks were observed to have reduced as a result of coordination which reduced the vibrational force of CO group upon coordination. This is further supported by variation in the positions of δ(C-O) deformation peaks in the complexes. The δ(C-O) deformation peak in the ligand appeared as a medium peak at 1339 cm⁻¹. The peak appeared as a weak peak at higher frequencies in Pt(II), Ni(II) and Mo(V) complexes. However, it appeared as a medium peak with lower frequencies in Mn(II) and Zn(II) complexes.

The azomethine group ν(C=N) band which appeared as a medium peak at 1610 cm⁻¹ in the spectrum of the ligand appeared at lower wavenumber in Mn(II), Zn(II) and Mo(V) complexes but at a slightly higher wavenumber in Pt(II) and Ni(II) complexes. However, δ(C-N) deformation mode for all the complexes was affected by coordination effect by shifting to higher wavenumber when compared to that of the ligand due to the coordination. The amide NH vibrational stretching mode appeared as a medium peak at 3266 cm⁻¹ in the spectrum of the hydrazone but could not be found in the metal complexes due to conjugation effect of the coordination of azomethine group to the central metal ions in the complexes.

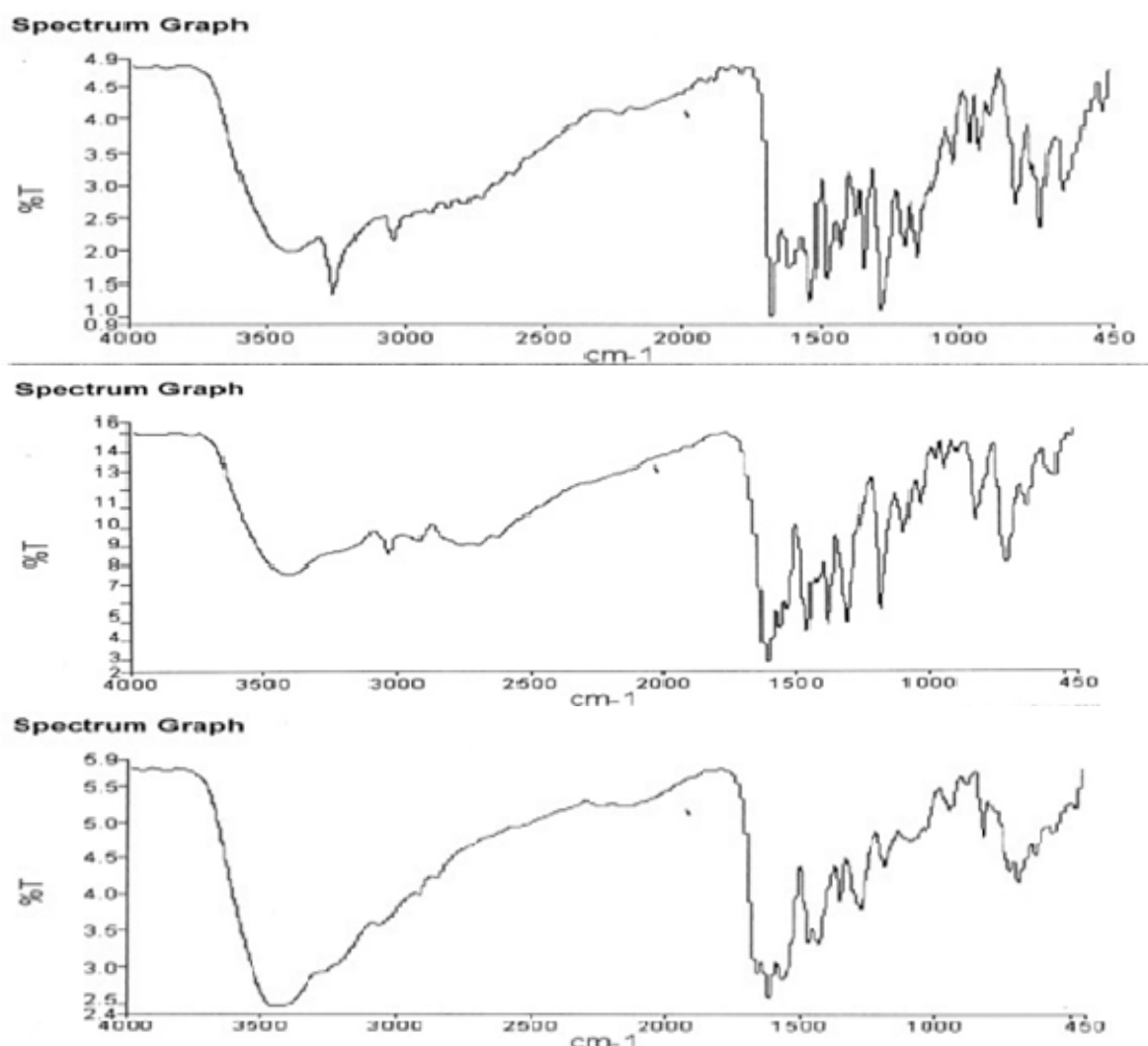


Fig. 5. Infrared spectra for H_2L^3 , Mn(II) and Pt(II) complex respectively.

Table 2. Infrared data of metal complexes of H_2L^3 .

Ligands/Complex	$\nu(OH)$ cm^{-1}	$\nu(C=O)$ cm^{-1}	$\nu(C=N)$ cm^{-1}	$\nu(N-N)$ cm^{-1}	$\delta(C-O)$ cm^{-1}	$\delta(C-N)$ cm^{-1}	(M-N) cm^{-1}	(M-O) cm^{-1}
H_2L^3 (1)	3418 s	1675vs	1610 m	1529 m	1339 m	1147 m	-	-
$[Mn(H_2L^3)(CH_3COO)_2]$ (2)	3411 m,b	1604w	1561 w	1467 m	1311 m	1153 m	631 w	520 w
$[Zn(H_2L^2)(CH_3COO)_2H_2O]$ (3)	3428 s,b	1611 m	1539 w	1427 w	1269m	1187 m	662 w	429 w
$[Pt(H_2L^3)Cl_2]$ (4)	3456 s,b	1655 w	1611 w	1470 m	1347 w	1184 m	625 w	455 w
$[Ni(H_2L^2)Cl_2]H_2O$ (5)	3402 s,b	1651m	1610 w	1566 m	1349 w	1184 m	554 w	477 w
$[Mo(H_2L^3)Cl_3]$ (6)	3419 s,b	1630 s	1538 w	1461 w	1346 w	1187 w	668 w	418 w

The assignment of the proposed coordination sites is further supported by the appearance of new bands between $554-668\text{ cm}^{-1}$ and $418-523\text{ cm}^{-1}$. They were assigned to M-N and M-O bands, respectively.

Electronic Spectra Study

The electronic spectral assignments of the metal complexes in methanol are presented in table 3. The interpretation was done on the basis of comparison of the

spectrum of the ligand with the spectral of the metal complexes. In a d^5 high spin Mn(II) complex, spin allowed d-d transition is not expected due to the fact that such transition are Laporte and spin forbidden (Mangalam *et al.*, 2009). Thus, for Mn(II) complex, the intensities of transition from ground state to the state of four-fold multiplicity are very weak as compared the ligand. However, the spectrum of the complex showed three significant intra-ligand transitions at ca. 43478, 36364 and

Table 3. Electronic data of H_2L^3 and its metal complexes.

Compound	Transition cm^{-1}	Ground Term Symbol	Transition
H_2L^3 (1)	46512	-	$\pi \rightarrow \pi^*$ (C=C) ar.
	34722		$n \rightarrow \pi^*$ (C=N)
	29326		$n \rightarrow \pi^*$ (C=O)
[Mn(H_2L^3)(CH_3COO) ₂] (2)	43478	6S	$\pi \rightarrow \pi^*$ (C=C) ar.
	36364		$n \rightarrow \pi^*$ (C=N)
	32680		$n \rightarrow \pi^*$ (C=O)
	23095		$^6A_1 \leftarrow ^6B_2$
[Zn(H_2L^3)(CH_3COO) ₂ H_2O] (3)	45454	5D	$\pi \rightarrow \pi^*$ (C=C) ar.
	33557		$n \rightarrow \pi^*$ (C=N)
	25974		$n \rightarrow \pi^*$ (C=O)
	17182		MLCT
[Pt(H_2L^3) ₂ .Cl] (4)	45662	3D	$\pi \rightarrow \pi^*$ (C=C) ar.
	34483		$n \rightarrow \pi^*$ (C=N)
	29240		$n \rightarrow \pi^*$ (C=O)
[Ni(H_2L^3) ₂ .Cl ₂]. H_2O (5)	45871	3F	$\pi \rightarrow \pi^*$ (C=C) ar.
	34602		$n \rightarrow \pi^*$ (C=N)
	29325		$n \rightarrow \pi^*$ (C=O)
	23981		MLCT
[Mo(H_2L^3) ₂ .Cl ₃] (6)	43290	7S	$n \rightarrow \pi^*$ (C=N)
	32258		$n \rightarrow \pi^*$ (C=O)
	24691		$^5T_{1g} \leftarrow ^7A_{1g}$
	16077		$^5T_{2g}(G) \leftarrow ^7A_{1g}$

32680 cm^{-1} . They were assigned to $\pi \rightarrow \pi^*$ of aromatic ring system, $n \rightarrow \pi^*$ of azomethine group and $n \rightarrow \pi^*$ of carbonyl group respectively. The complex showed a high intense transition at visible region due to ligand to metal charge transfer (LCMT) transition. It was assigned to $^2A_1 \leftarrow ^2B_2$ transition. This observation is of the characteristic of the tetrahedral pyramidal geometry. Zn(II) ion is of d^{10} configuration, therefore, $d-d$ transitions are not expected in the complexes. The intra-ligand transitions appeared in the complexes at higher wavelength with low intensities due to coordination effect on the chromophoric group. However, a very weak shoulder peak, which is attributed to metal-ligand charge transfer, is observed at ca. 17182 cm^{-1} perhaps, because of the yellow colour of the complex (Mohareb *et al.*, 2011). Pt(II) is of d^9 configuration with term symbol 3D . Therefore, only one $d-d$ transition is expected. However, the spectrum of the complex showed only three significant transitions at ca. 45662, 34483 and 29240 cm^{-1} in the region studied. They were attributed to intra-ligand transitions. The transitions experienced slight shift due to coordination effect.

Ni(II) complex spectrum showed three bands attributed to intra-ligand transitions at ca. 45871, 34602 and 29325 cm^{-1} . However, absence of peak below 16000 cm^{-1} ruled out the possibility of tetrahedral geometry. The magnetic value, 3.53 BM, obtained supported distorted octahedral geometry. The low intense peak at ca. 23981 cm^{-1} in the

visible region of the spectrum is attributed to ligand-metal charge transfer (LCMT) in the complex.

Mo(V) is of d^5 configuration with term symbol 7S , The spectrum of the complex consists of weak spin-forbidden bands at ca. 24691 and 16077 cm^{-1} . The $d-d$ transition from this high spin d^5 configuration complex is possible due to pairing of some electron parallel spins in the complex. Using the Orgel diagram, the bands were assigned to transitions $^5T_{1g} \leftarrow ^7A_{1g}$ and $^5T_{2g}(G) \leftarrow ^7A_{1g}$ transition. However, the two bands at ca. 43290 and 32258 cm^{-1} were assigned to intra-ligand bands. The band at ca. 46512 cm^{-1} in the spectrum of the ligand could not be traced to metal complex, thus suggesting distorted geometry for the complex.

TGA/DTA Analyse

TGA and DTA curves obtained for Mn(II) and Ni(II) and complexes within the temperature range from ambient temperature up to 700°C in an inert atmosphere are as shown in Fig. 6. The curve for Mn(II) complex shows that the compound was very stable from ambient temperature up to 339°C. However, the compound decomposed in two steps at 348 and 427°C as shown in the DTG peaks. The H_2L^3 ligand constitute 60% of the complex but only 50% weight loss was observed in the first decomposition step between 339-417 °C. The second decomposition step which occurred between 417-440 °C

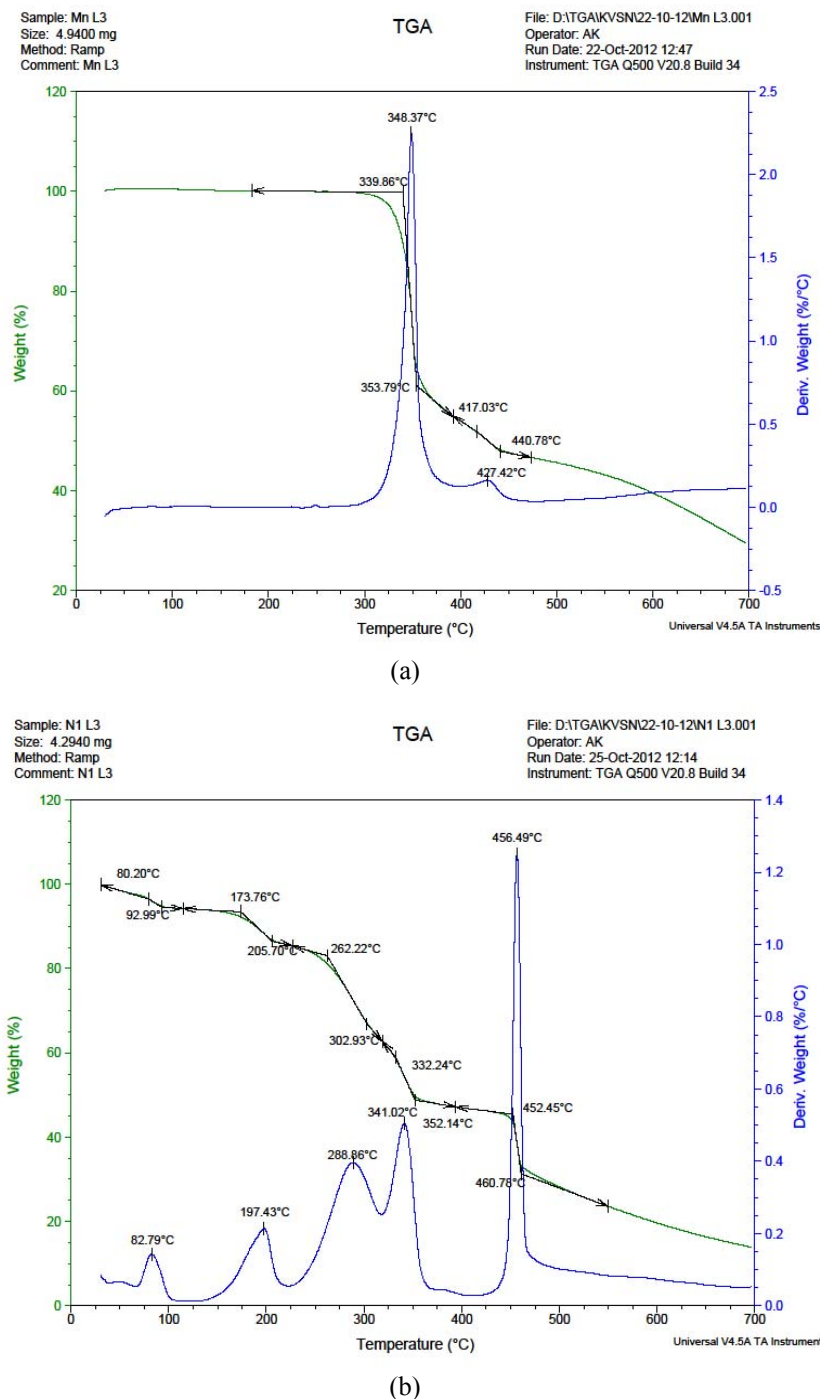


Fig. 6. TGA/DTA spectrum for Mn(II) and Ni(II) complex respectively.

corresponds to 10% (Cald. 9.9%) weight loss. This was attributed to decomposition of CH_3CO from the coordinated CH_3COO group. The residue at 440°C contained 10% of the H_2L^3 ligand. Thus, the complex did not fully decompose at the temperature range studied. Nevertheless, the thermogram was useful in predicting the structure of the complex (Munde *et al.*, 2012; Artur *et al.*, 2013). The TG and DTG curves for Ni(II) complex

proceeded with five degradation steps which occurred at 82 , 197 , 288 , 341 and 456°C . The first step decomposition occurred with the loss of lattice water outside the coordination sphere at the temperature range of 80 - 92°C and this corresponded to 4% weight loss. The second and the fourth decomposition steps occurred within the temperature range of 173 - 205 and 332 - 352°C and accounted for 8% loss each which is attributed to the loss

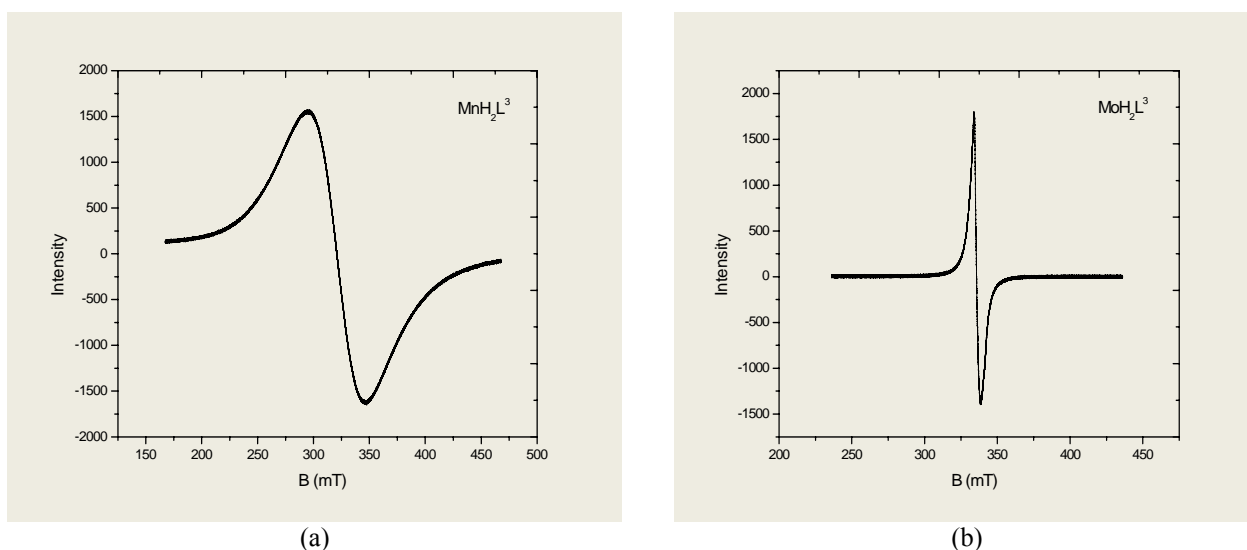


Fig. 7. EPR spectrum for $[\text{Mn}(\text{H}_2\text{L}^3)_2(\text{CH}_3\text{COO})_2]$ and $[\text{Mo}(\text{H}_2\text{L}^3)_2\text{Cl}_2]$ respectively in DMSO at 77 K.

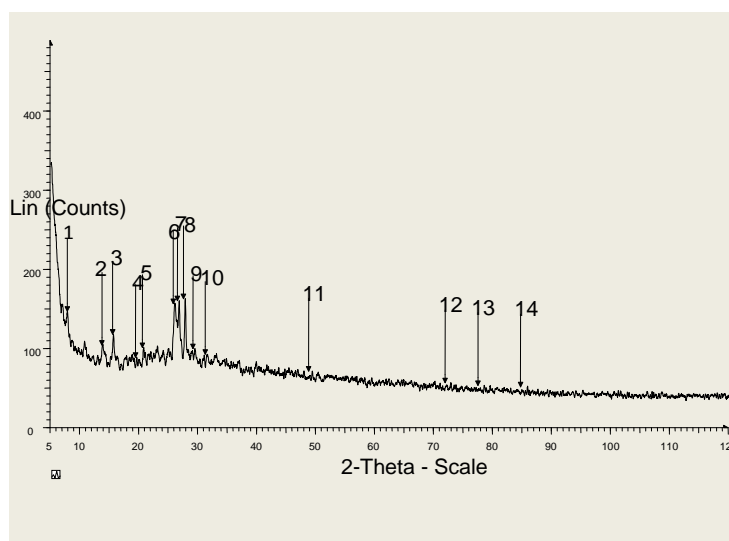


Fig. 8. X-ray diffraction pattern for $[\text{Ni}(\text{H}_2\text{L}^3)\text{Cl}_2]\cdot\text{H}_2\text{O}$.

of coordinated chlorine atoms in the complex. The decompositions which occurred within 262–302°C and 352–460°C were attributed to decomposition of H_2L^3 ligand. The decompositions accounted for 17% and 39% weight loss respectively. Thereafter, the compound decomposed to residue which is about 24% of the compound.

Electron Paramagnetic Resonance Spectra

The EPR spectra for Mn(II) and Mo(V) complexes recorded in DMSO at liquid nitrogen temperature are as shown in figure 7. Electron paramagnetic resonance spectrum of $[\text{Mn}(\text{H}_2\text{L}^3)_2(\text{CH}_3\text{COO})_2]$ displayed one broad spectrum with no hyperfine splitting, which could be as a result of large D value i.e the axial zero field splitting for

the complex as indicated in the spin Hamiltonian for manganese(II).

$$\hat{H} = g\beta H_s + D\{S_z^2 - 1/3S(S+1)\} + E(S_x^2 - S_y^2)$$

However, the observed $g_{av} = 2.0361$ value was found to be very close to the free electron spin value, 2.0023 which is consistent with the typical manganese (II) and also suggestive of the absence of spin orbital coupling in the ground state 6A_1 . The other g values are $g_{\parallel} = 3.7080$ and $g_{\perp} = 1.9842$. The fact that $g_{\parallel} > g_{\perp}$ favoured octahedral geometry for the complex but the magnetic values obtained proposed distorted geometry which is an indication that one corner of the complex was occupied by lone pair of electron.

The X-band EPR spectrum of $[\text{Mo}(\text{H}_2\text{L}^3)\text{Cl}_3]$ is characterized by only a single line with no hyperfine

Table 4. Powder X-ray data of $[\text{Ni}(\text{H}_2\text{L}^3)\text{Cl}_2]\text{H}_2\text{O}$.

Peak	$2\theta^\circ$	$d_{\text{obs}}(\text{Å})$	IntensityCount	Intensity %	$(1/d^2)$	$(1/d^2)/Z$	h	k	l
1	7.776	11.3607	147	90.3	0.00775	1	1	0	0
2	13.662	6.47613	104	63.7	0.02384	3	1	1	1
3	15.477	5.72079	117	72.3	0.03056	4	2	0	0
4	19.377	4.57718	88	54.2	0.04773	6	2	1	1
5	20.521	4.32457	100	61.8	0.05327	8	2	2	0
6	25.765	3.45499	156	96.1	0.08377	11	3	1	1
7	26.469	3.36471	160	98.4	0.08833	11	3	1	1
8	27.493	3.24158	163	100	0.09517	12	2	2	2
9	29.124	3.06367	99.2	61	0.1065	14	3	2	1
10	31.195	2.8649	91.9	56.6	0.1218	16	4	0	0
11	48.765	1.86593	70.6	43.4	0.08255	10	3	1	0
12	71.96	1.31114	55.9	34.4	0.5817	75	2	2	0
13	77.556	1.22992	52.5	32.3	0.661	85	3	0	0
14	84.784	1.14254	50.6	31.1	0.7661	99	3	1	0

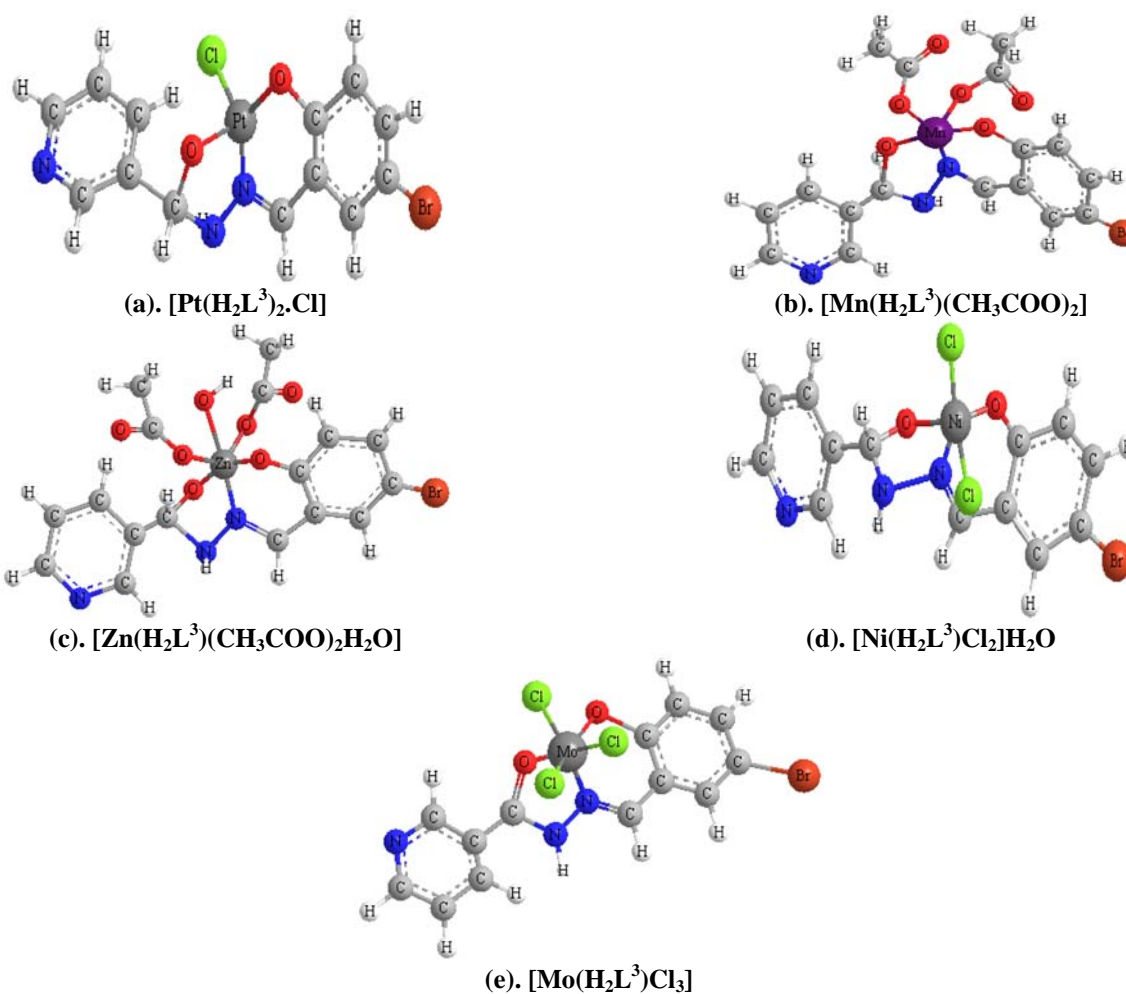
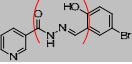
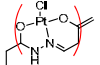
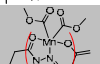
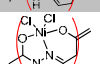
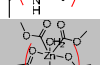


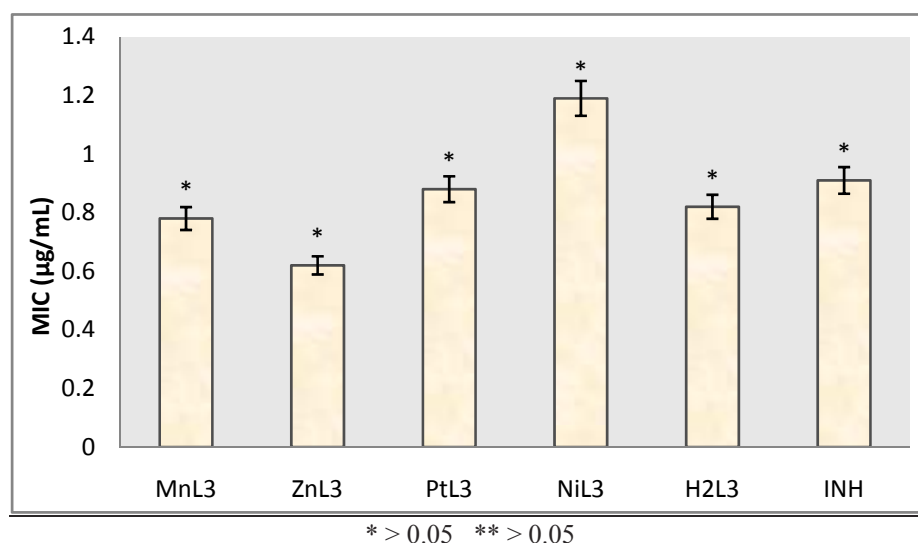
Fig. 9. Proposed structures of (a): $[\text{Pt}(\text{H}_2\text{L}^3)_2\cdot\text{Cl}]$, (b): $[\text{Mn}(\text{H}_2\text{L}^3)(\text{CH}_3\text{COO})_2]$, (c): $[\text{Zn}(\text{H}_2\text{L}^3)(\text{CH}_3\text{COO})_2\cdot\text{H}_2\text{O}]$, (d): $[\text{Ni}(\text{H}_2\text{L}^3)\text{Cl}_2]\cdot\text{H}_2\text{O}$ and (e): $[\text{Mo}(\text{H}_2\text{L}^3)\text{Cl}_3]$

splitting. However, the EPR parameters were found to satisfy the octahedral geometry. The g_{iso} value = 1.9537 support the monomeric nature of the complex (Wood *et*

al., 1996; Pilbrow, 1990). The $g_{\parallel} = 2.5138$ while $g_{\perp} = 1.9537$, which is of characteristic of octahedral geometry.

Table 5. MIC ($\mu\text{g/mL}$), IC_{50} (μM) and SI ($\text{IC}_{50}/\text{MIC}$) values of the metal complexes of H_2L^3 .

Entry	Compound	MIC ($\mu\text{g/mL}$)	IC_{50} (μM)	SI ($\text{IC}_{50}/\text{MIC}$)
H_2L^3		0.82 ± 0.016	2.25	2.74
PtL3		0.88 ± 0.033	2.19	2.19
MnL3		0.78 ± 0.062	0.92	1.30
NiL3		1.19 ± 0.194	1.21	1.83
ZnL3		0.62 ± 0.031	1.34	1.34
INH	-	0.91 ± 0.133	-	-

Fig. 10. Comparing MIC ($\mu\text{g/mL}$) values of the metal complexes of H_2L^3 with the ligand (H_2L^3) and isoniazid (INH) drug.

Powder X-ray diffraction study

X-ray powder diffraction pattern for Ni(II) complex recorded on a Bruker AXS D8 Advance diffractometer operating in the $\theta:\theta$ mode, equipped with a secondary beam graphite monochromator is as shown in (Fig. 8). The diffractogram of Ni(II) complex consists of fourteen reflections in the range of 7.776–84.784 (2θ value) with maxima at $2\theta = 9.294^\circ$. The major peaks of relative intensity greater than 10% were indexed using a computer programme (Table 4) (Nomiya *et al.*, 2004; Lipson, 1949). This indexing method also yields the Miller indices (hkl), the unit cell parameters and the unit cell volume. The unit cell of Ni(II) complex yielded values of lattice constants: $a = 12.868 \text{ \AA}$ and $c = 22.154 \text{ \AA}$, and a unit cell volume $V = 3176.909 \text{ \AA}^3$ which is in consistency with trigonal parameters. The conditions satisfied trigonal samples with conditions such as $a = b \neq c$ and $\alpha = \beta = 90^\circ$; $\gamma = 120^\circ$. Hence, it can be concluded $[\text{Ni}(\text{H}_2\text{L}^3)\text{Cl}_2]\text{H}_2\text{O}$ complexes was trigonal bipyramidal crystal systems.

Based on the analytical and spectroscopic data obtained, the modeling structures for the metal complexes of H_2L^3 synthesized are shown in figure 9:

Antimycobacterial study

The antitubercular efficacy of the hydrazone and the metal complexes except that of Mo(V) complex were determined by screening them against *Mycobacterium tuberculosis H37Rv*. (ATCC 35837). Minimum inhibitory concentrations (MIC) were determined by microbroth dilution in accordance with the methods of the National Committee for Clinical Laboratory Standards (NCCLS) as described earlier (Anna *et al.*, 2009; Koen Andries *et al.*, 2005) and MIC's are given in Table 5. Standard drugs, isoniazid was used as positive control while DMSO was used as solvent.

The MIC results for the ligand, H_2L^3 (Table 5; Fig. 10) was compared to four of its transition metal complexes. The MIC's result illustrates that H_2L^3 exhibited promising anti-tubercular activity with MIC value of 0.82 $\mu\text{g/mL}$ compared to isoniazid (0.91 $\mu\text{g/mL}$). Also, metal complexes with coordinated methoxyl group (MnL3 and ZnL3) showed higher activity than isoniazid with MIC value of 0.78 and 0.62 $\mu\text{g/mL}$ respectively. The two complexes exhibited anti-tubercular potency than the standard drug. The potency of the compounds observed could be attributed to coordination ligand to metal ion, as well as the presence of OCH_3 substituent in the molecule of the complexes. However, PtL3 complex (0.88 $\mu\text{g/mL}$) with one coordinated chlorine atom was found to be more active than complex NiL3 complex (1.19 $\mu\text{g/mL}$) with two coordinated chlorine atoms. Thus, NiL3 complex was found with reduction in inhibition potential. Generally, the results indicate that MnL3 and ZnL3 are more potent than the hydrazone and Isoniazid with low toxicity. This observation was supported with the test of significant which indicated that $P < 0.05$ for all the complexes. However, PtL3 was found with highest toxicity with IC_{50} value of 1.93 μM .

CONCLUSION

In conclusion, an acylhydrazone was successfully synthesized from nicotinic hydrazide by cold condensation reaction. The hydrazone formation was confirmed by one and two dimensional NMR techniques. The novel metal complexes of the hydrazone were successfully synthesized. The structures of the metal complexes were elucidated on the basis of analytical data, ESR, magnetic measurement, DTA/TGA and powder X-ray study. All the efforts made to grow single crystals of the metal complexes did not yield positive results. The anti-tubercular efficacies of the compounds were established. The hydrazone (H_2L^3) and some of the metal complexes (MnL3, ZnL3 and PtL3) were found to possess better activity as compared to isoniazid.

ACKNOWLEDGEMENT

We gratefully acknowledge the financial support of CISR and TWAS through TWAS-CSIR fellowship. We thank technical staff of Sophisticated Analytical Instrument Facility at Central Drug Research Institute, Lucknow; Indian Institute of Technology, Roorkee and Indian Institute of Technology, Bombay, India for technical support.

REFERENCES

Abeda, J., Anne, K., Duhme, K., Kiranmayi, V., Manjula, S., Prasad, D. and Subhash, P. 2012. Synthesis, characterisation and antitubercular activities of a series of

pyruvate-containing aroylhydrazones and their Cu-complexes. Dalton Trans. 41:91-92.

Aboul-Fadl, T., Bin-Jubair, FAS. and Aboul-Wafa, O. 2010. Schiff bases of indoline-2,3-dione (isatin) derivatives and nalidixic acid carbohydrazide, synthesis, antitubercular activity and pharmacophoric model building. Eur. J. of Med. Chem. 45:4578-4586.

Andreani, A., Burnelli, S., Granaiola, M., Leoni, A., Locatelli, A., Morigi, R., Rambaldi, M., L. Varoli, Calonghi, N., Cappadone, C., Farruggia, G., Zini, M. Stefanelli, C., Masotti, L., Radin, NS. and Shoemaker, RH. 2008. New antitumor imidazo[2,1-b]thiazole guanylhyazones and analogues. J. Med. Chem. 51(4):809-816.

Anna, CH., Rooda, A., Marijke, JW., Klaas, KB., Karen, V., Jerome, G., Koen, A., Holger, L., Anil, K. and Dirk, B. 2009. Selectivity of TMC 207 towards *Mycobacterial* ATP Synthase Compared with That towards the Eukaryotic Homologue. Antimicrob. Agents Chemother. 53(3):1290.

Artur, RS., Wałęsa-Chorab, M., Harro wfield, J., Kubicki, M., Zbigniew, H., Korabik, M. and Patroniak, V. 2013. Self-assembly of transition metal ion complexes of a hybrid pyrazine-terpyridine ligand. Dalton Trans. 42:1743-1751.

Banerjee, S., Mondal, S., Chakraborty, W., Sen, S., Gachhui, R., Butcher, RJ., Slawin, C. Mandal, AMZ. and Mitra, S. 2009. Syntheses, X-ray crystal structures, DNA binding, oxidative cleavage activities and antimicrobial studies of two Cu(II) hydrazone complexes. Polyhedron. 28:2785-2793.

Davidson, G. 2010. Spectroscopic Properties of Inorganic and Organometallic Compounds. Royal Society of Chemistry. 39:12-226.

Devidas, SM., Quadri, SH., Kamble, SH., Syed, FM. and Vyavhare, DY. 2011. Novel One-Pot Synthesis of Schiff Base Compounds Derived From Different Diamine and Aromatic Aldehyde Catalyzed by $\text{P}_2\text{O}_5/\text{SiO}_2$ Under Free-Solvent Condition at Room Temperature. J. Chem. Pharm. Res. 3(2):489-495.

Dharmaraj, N., Sathyadevi, P., Krishnamoorthy, P., Alagesan, M., Thanigaimani, K. and Thomas, MP. 2012. Synthesis, crystal structure, electrochemistry and studies on protein binding, antioxidant and biocidal activities of Ni(II) and Co(II) hydrazone complexes. Polyhedron. 31: 294-306.

Dover, LG. and Coxon, GD. 2011. Current status and research strategies in tuberculosis drug development. J. Med. Chem. 54:6157-6165.

Gopalakrishnan, A., Shanmugasundaram, A., Nanjundan, AK., Jong, TK., Kwon, T., Senthamaraiannan, K. and Yeon, TJ. 2008. A facile synthesis, antibacterial, and

- antitubercular studies of some piperidin-4-one and tetrahydropyridine derivatives. *Bioorganic and Medicinal Chemistry Letters*. 18:6542-6548.
- Harper, C. 2009. Tuberculosis, a neglected opportunity? *Nat. Med.* 13: 309-312.
- Jia, L., Tomaszewski, JE., Hanrahan, C., Coward, L., Noker, P., Gorman, G., Nikonenko, B. and Protopopova, M. 2005. Pharmacodynamics and pharmacokinetics of SQ109, a new diamine-based antitubercular drug. *British J. Pharmacol.* 144:80-87.
- Jindani, A., Nunn, AJ. and Enarson, DA. 2004. Two 8-month regimens of chemotherapy for treatment of newly diagnosed pulmonary tuberculosis: International multicentre randomised trial. *Lancet*. 364:1244-1251.
- Kaufmann, SHE. and Parida, SK. 2008. Tuberculosis in Africa: Learning from pathogenesis for biomarker identification. *Cell Host Microb.* 4:219-228.
- Koen Andries, K., Verhasselt, P., Guillemont, J., Göhlmann, HWH., Jean-Marc, N., Winkler, H., Gestel, JV., Timmerman, P., Zhu, M., Ennis, L., Williams, P., Chaffoy, D., Huitric, E., Hoffner, S., Cambau, E., Truffot-Pernot, C., Lounis, N. and Vincent, JV. 2005. A Diarylquinoline Drug Active on the ATP Synthase of *Mycobacterium tuberculosis*. *Science*. 307(5707):223-227.
- Kuriakose, M., Kurup, MRP. and Suresh, E. 2007. Spectral characterization and crystal structure of 2-benzoylpyridine nicotinoyl hydrazone. *Spectrochim Acta. Mol Biomol Spectrosc.* 66(2): 353-358.
- Laughon, BE. 2007. New tuberculosis drugs in development. *Curr. Topics Med. Chem.* 7:463-473.
- Lipson H. 1949. *Acta Crystallog.* 2:24-43.
- Lourenço, MCDS., Ferreira, MDL., De Souza, MVN., Peralta, MA., Vasconcelos, TRA. and Henriques, MDO. 2008. Synthesis and anti-mycobacterial activity of (*E*)-*N'*-(monosubstituted benzylidene) isonicotinohydrazide derivatives. *Eur. J. Med. Chem.* 43:1344-1347.
- Mangalam, NA., Sivakumar, S., Sheeja, SR., Kurup, MRP. and Tiekink, RT. 2009. Chemistry of molecular and supramolecular structures of vanadium(IV) and dioxxygen-bridged V(V) complexes incorporating tridentate hydrazone ligands. *Inorg. Chim. Acta.* 362:4191-4197.
- Mohareb, RM, Daisy, HF. and Sakka, OK. 2011. Novel Synthesis of Hydrazone-Hydrazone Derivatives and Their Utilization in the Synthesis of Coumarin, Pyridine, Thiazole and Thiophene Derivatives with Antitumor Activity. *Molecules*. 16:16-27.
- Munde, AS., Shelke, VA., Jadhav, SM., Kirdant, AS., Vaidya, SR., Shankarwar, SG. and Chondhekar, TK. 2012. Synthesis, Characterization and Antimicrobial Activities of some Transition Metal Complexes of Biologically Active Asymmetrical Tetradentate Ligands. *Adv. Appl. Sci. Res.* 3(1):175-182.
- Nair, Y., Sithambaresan, MM. and Kurup, MRP. 2012. *N'*-[(*E*)-(3-Fluoropyridin-2-yl)methylidene]benzohydrazide monohydrate. *Acta Crystallogr. Struct Rep Online. Sect. E68(9)*. doi: 10.1107/S1600536812035179.
- Nomiya, K., Yoshizawa, A., Tsukagoshi, K., Kasuga, NC., Hirakawa, S. and Watanabe, J. 2004. Synthesis and structural characterization of silver(I), aluminium(III) and cobalt(II) complexes with 4-isopropyltropolone (hinokitil) showing noteworthy biological activities. Action of silver(I)-oxygen bonding complexes on the antimicrobial activities. *J. Inorg. Biochem.* 98(1):46-60.
- Parekh, J., Inamdhar, P., Rathish, N., Shipra, B. and Sumitra, C. 2005. Synthesis and antibacterial activity of some Schiff bases derived from 4-aminobenzoic acid. *J. Serb. Chem. Soc.* 70(10):1155-1161.
- Pavia, DL., Lampman, GM., Kriz, GS. and Vyvyan, JA. 2008. Introduction to Spectroscopy. Brooks Cole. (4th edi.)1-312.
- Pilbrow, JR., 1990. Transition Ion Electron Paramagnetic Resonance. Clarendon Press, Oxford. 12-89.
- Rakesh, SD., Lee, RB., Tangallapally, RP. and Lee, RE. 2009. Synthesis, optimization and structure activity relationships of 3,5-disubstituted isoxazolines as new anti-tuberculosis agents. *Eur. Med. Chem.* 9:809-840.
- Ramon-Garcia, S., Ng, C., Anderson, H., Chao, JD., Zheng, X., Pfeifer, T., Av-Gay, Y., Roberge, M. and Thompson, CJ. 2011. Synergistic drug combinations for tuberculosis therapy identified by a novel highthroughput screen. *Antimicrob. Agents Chemother.* 55:3861-3869.
- Rollas, S. and Kucukguzel, SG. 2007. Biological Activities of Hydrazone Derivatives. *Molecules*. 12(8):1910-1939.
- Sacchetti, JC., Rubin, EJ. and Freundlich, JS. 2008. Drugs versus bugs: in pursuit of the persistent predator *Mycobacterium tuberculosis*. *Nat. Rev. Microbiol.* 6:41-52.
- Salib, KA., Iskak, MF., El-Behairy, M. and Abd El-Halim, HF. 2003. Synthesis, spectroscopic studies of a novel Schiff base Derived from *o*-acetoacetylphenol and ethylamine and its metal complexes. *Synth. React. Inorg. Met.-Org. Chem.* 33:1667-1687.
- Shi, L., Ge, HM., Tan, SH., Li, HQ., Song, YC. and Zhu, HL. 2007. Synthesis and antimicrobial activities of Schiff bases derived from 5-chloro-salicylaldehyde. *Eur. J. Med. Chem.* 42(4):558-564.
- Wood, RM., Stucker, DM., Jones, LM., Lynch, WB., Sushil, KM. and Freed, JH. 1996. An EPR Study of Some

Highly Distorted Tetrahedral Manganese (II) Complexes at High Magnetic Fields. *Inorg. Chem.* 38:5384-5388.

World Health Organization (WHO). 2010. Tuberculosis-fact sheet. Geneva. No. 104:1-3.

Received; Jan 6, 2015; Revised and Accepted: March 4, 2015